

High efficient Raman sideband cooling and strong three-body recombination of atoms

Yuqing Li(李玉清), Zhennan Liu(刘震南) Yunfei Wang(王云飞) Jizhou Wu(武寄洲), Wenliang Liu(刘文良), Yongming Fu(付永明) Peng Li(李鹏) Jie Ma(马杰), Liantuan Xiao(肖连团), and Suotang Jia(贾锁堂)
Citation: Chin. Phys. B, 2023, 32 (**10**): 103701. DOI: 10.1088/1674-1056/acec42
Journal homepage: http://cpb.iphy.ac.cn; http://iopscience.iop.org/cpb

What follows is a list of articles you may be interested in

Quantum degenerate Bose-Fermi atomic gas mixture of ^{23}Na and ^{40}K

Ziliang Li(李子亮), Zhengyu Gu(顾正宇), Zhenlian Shi(师振莲), Pengjun Wang(王鹏军), and Jing Zhang(张靖)
Chin. Phys. B, 2023, 32 (**2**): 023701. DOI: 10.1088/1674-1056/aca14f

Space continuous atom laser in one dimension

Yi Qin(秦毅), Xiao-Yang Shen(沈晓阳), Wei-Xuan Chang(常炜玄), and Lin Xia(夏林)
Chin. Phys. B, 2023, 32 (**1**): 013701. DOI: 10.1088/1674-1056/ac7861

Superfluid to Mott-insulator transition in a one-dimensional optical lattice

Wenliang Liu(刘文良), Ningxuan Zheng(郑宁宣), Jun Jian(蹇君), Li Tian(田丽), Jizhou Wu(武寄洲), Yuqing Li(李玉清), Yongming Fu(付永明), Peng Li(李鹏), Vladimir Sovkov, Jie Ma(马杰), Liantuan Xiao(肖连团), and Suotang Jia(贾锁堂)
Chin. Phys. B, 2022, 31 (**7**): 073702. DOI: 10.1088/1674-1056/ac6579

Enhanced cold mercury atom production with two-dimensional magneto-optical trap

Ye Zhang(张晔), Qi-Xin Liu(刘琪鑫), Jian-Fang Sun(孙剑芳), Zhen Xu(徐震), and Yu-Zhu Wang(王育竹)
Chin. Phys. B, 2022, 31 (**7**): 073701. DOI: 10.1088/1674-1056/ac5397

Efficient loading of ultracold sodium atoms in an optical dipole trap from a high power fiber laser

Jing Xu(徐静), Wen-Liang Liu(刘文良), Ning-Xuan Zheng(郑宁宣), Yu-Qing Li(李玉清), Ji-Zhou Wu(武寄洲), Peng Li (李鹏), Yong-Ming Fu(付永明), Jie Ma(马杰), Lian-Tuan Xiao(肖连团), and Suo-Tang Jia(贾锁堂)
Chin. Phys. B, 2021, 30 (**3**): 033701. DOI: 10.1088/1674-1056/abc678

RAPID COMMUNICATION

High efficient Raman sideband cooling and strong three-body recombination of atoms

Yuqing Li(李玉清)[1,2], Zhennan Liu(刘震南)[1], Yunfei Wang(王云飞)[1], Jizhou Wu(武寄洲)[1,2,†], Wenliang Liu(刘文良)[1,2], Yongming Fu(付永明)[1], Peng Li(李鹏)[1], Jie Ma(马杰)[1,2], Liantuan Xiao(肖连团)[1,2], and Suotang Jia(贾锁堂)[1,2]

[1] *State Key Laboratory of Quantum Optics and Quantum Optics Devices, Institute of Laser Spectroscopy, College of Physics and Electronics Engineering, Shanxi University, Taiyuan* 030006, *China*

[2] *Collaborative Innovation Center of Extreme Optics, Shanxi University, Taiyuan* 030006, *China*

(Received 28 May 2023; revised manuscript received 22 July 2023; accepted manuscript online 1 August 2023)

We report a highly efficient three-dimensional degenerated Raman sideband cooling (3D dRSC) that enhances the loading of a magnetically levitated optical dipole trap, and observe the strong atom loss due to the three-body recombination. The 3D dRSC is implemented to obtain 5×10^7 Cs atoms with the temperature of ~ 480 nK. The cold temperature enables 1.8×10^7 atoms loaded into a crossed dipole trap with an optimized excessive levitation magnetic gradient. Compared to the loading of atoms from a bare magneto-optical trap or the gray-molasses cooling, there is a significant increase in the number of atoms loaded into the optical dipole trap. We derive for the three-body recombination coefficient of $L_3 = 7.73\times10^{-25}$ cm^6/s by analyzing the strong atom loss at a large scattering length of 1418 Bohr radius, and discover the transition from the strong three-body loss to the dominant one-body loss. Our result indicates that the lifetime of atoms in the optical dipole trap is finally decided by the one-body loss after the initial strong three-body loss.

Keywords: matter wave, atom cooling methods, ultracold gases

PACS: 37.10.De, 03.75.–b, 67.85.–d **DOI:** 10.1088/1674-1056/acec42

1. Introduction

Laser cooling and trapping techniques enable the preparation and application of atomic ensembles at ultracold temperatures, where many quantum effects will dominate.[1–7] As a kind of sub-Doppler cooling, gray molasses has been demonstrated as a powerful tool to cool the atomic sample to a lower temperature for ^{6}Li,[8–10] ^{7}Li,[11] ^{23}Na,[12,13] ^{39}K,[14,15] ^{40}K,[9,16] ^{41}K,[17] ^{87}Rb[18] and ^{133}Cs atoms[19] than the general optical molasses cooling. In a different approach, three-dimensional degenerated Raman sideband cooling (3D dRSC) was earlier used to obtain sub-μK temperature in the pioneering works on Cs atoms.[20,21] 3D dRSC is also indispensable for Cs atoms to achieve their atomic Bose–Einstein condensate.[22–25] Quite recently, 3D dRSC has been used for ^{39}K atoms and produces a lower temperature of $T = 1.3$ μK compared to the result from the gray molasses cooling.[26] For the ^{87}Rb and ^{133}Cs atoms trapped in a 2D optical lattice operating at the wavelength of $\lambda = 1064$ nm, dRCS enables the production of quantum gases by the direct laser cooling.[27,28]

Since dRSC is used to cool the atomic sample to a low temperature around 1 μK, a large volume optical dipole trap (ODT) with the shallow trapping potential is beneficial to enhance the number of atoms loaded into the ODT.[29–31] For the interacting ultracold Bose atoms in the ODT, of particular interest is the three-body recombination, in which two particles form a dimmer while interacting with a third particle. Understanding the three-body recombination has for a long time been important in the studies of both few- and many-body physics in ultracold atoms.[32] The universal scaling laws in the strongly correlated unitary Bose gases dominated by the three-body recombination have been explored experimentally and theoretically.[33–36] For the non-degenerated ultracold Bose atoms at the large scattering length, the three-body recombination induces the large atom loss and heating.[37–39] Thus, a highly efficient 3D dRSC is promised for the preparation of a large number of atoms in the optical dipole trap, and a comprehensive study of the three-body recombination is significant for understanding the unequilibrium process after loading of cooled atoms into the optical dipole trap.

In this work, we realize a highly efficient 3D dRSC for Cs atoms and obtain an ultracold temperature of $T \sim 500$ nK. The cold temperature is consistent with the theoretical estimation according to the calibrated energy spacing of neighboring vibrational levels in the lattice used in 3D dRSC. Combined with the optimized excessive levitation gradient, the cold temperature enables a large number of atoms to be loaded into the magnetically levitated ODT. The evolution of the number of atoms trapped in the ODT is measured at a large scattering length, and a strong three-body loss is observed. The three-body recombination coefficient is obtained by fitting the derived model to the data. In particular, the one-body loss due

†Corresponding author. E-mail: wujz@sxu.edu.cn

© 2023 Chinese Physical Society and IOP Publishing Ltd

to the collisions of atoms with background gas becomes dominant after the large reduction of atomic density under the initial strong three-body loss.

2. Experimental setup and process

The experimental scheme of 3D dRCS is basically the same as the previous works on Cs atoms.[20,21,27,28] The main difference is the geometric configuration of the lasers constructing the lattice and the optical pumping laser. As shown in Fig. 1, a stable 3D lattice is formed by using one retroreflected standing wave and two running waves. The standing wave has an angle of $\sim 77^\circ$ with the vertical direction, and is perpendicular to another beam with an angle of $\sim 13^\circ$ relative to the horizontal plane. The linear polarizations of the two running beams lie in a plane, which is formed by these two running beams. The two polarizations of the standing wave are rotated by $\pm 10^\circ$ relative to the angular bisector of the two running beams. This special polarization configuration of four laser beams guarantees the maximum of the Raman coupling in 3D dRSC. The optical pump laser is calibrated to a σ^+ polarization and reflected by a mirror. The magnetic field is optimized to mainly parallel to the optical pump laser beam.

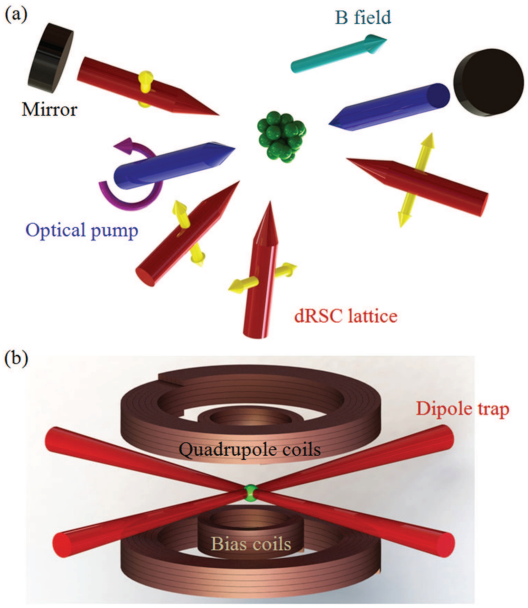


Fig. 1. Experimental geometry and configuration of both lasers and magnetic coils for the 3D dRSC and the magnetic levitated loading of ODT. (a) The lattice (red inward arrows) consists of two running laser beams with the polarizations that lie in the plane determined by these two beams and the retro-reflected standing wave with the $\pm 10^\circ$ polarizations (yellow arrows) relative to the angular bisector of the two running beams. The optical pump laser (blue arrows) has the σ^+ polarization and reflected by a mirror. The direction of the combined magnetic field is mainly parallel with the optical pump laser beam. (b) The magnetically levitated ODT consists of a pair of quadrupole coils in anti-Helmholtz configuration, a pair of bias coils in Helmholtz configuration, and two horizontally crossing 1064-nm laser beams at an angle of $\sim 90^\circ$.

The lattice lasers are derived from a power-amplified external-cavity diode laser (ECDL), which is operated without the frequency stabilization. The frequency is tuned to a red detuning of $\Delta_l = -22$ GHz from the $6S_{1/2}$, $F = 3 \rightarrow 6P_{3/2}$, $F' = 4$ transition of Cs atoms. The standing wave laser has the power of ~ 46 mW, and the other two running lasers have the same power of ~ 16.5 mW. A weak magnetic field, which is used to bring the vibrational sublevel $|n\rangle$ in the $|F = 3, m_F\rangle$ state to degeneracy with the vibrational sublevel $|n-1\rangle$ in the $|F = 3, m_F - 1\rangle$ state, is provided by the combined field of three pairs of compensation coils. This magnetic field is optimized by minimizing the atomic temperature and maximizing the number of atoms after 3D dRSC. The optical pumping laser with the power of ~ 1.2 mW is from another ECDL, which provides the repumping laser in the magneto-optical trap (MOT), and is detuned by $+10$ MHz from the $6S_{1/2}$, $F = 3 \rightarrow 6P_{3/2}$, $F' = 2$ transition. An additional depumping laser is introduced to pump the atoms back to the $F = 3$ ground state, since the excited atoms in 3D dRSC can decay to the $F = 4$ ground state, in which the atoms can't participate in the cooling process. Here the cooling laser in MOT is used for the depumping laser and is detuned by $+10$ MHz relative to the $6S_{1/2}$, $F = 4 \rightarrow 6P_{3/2}$, $F' = 4$ transition.

After 3D dRSC, we use a large-volume crossed ODT with the shallow potential of $\sim k_B \times 9$ μK to capture more atoms, where k_B is the Boltzmann constant. The ODT consists of two horizontally crossing 1064-nm laser beams at an angle of $\sim 90^\circ$. These two beams have the same power of ~ 2 W, and the beam waists are $w_x = 310 \pm 12$ μm and $w_y = 300 \pm 13$ μm. During the loading of ODT, the large gravity of Cs atom induces a big destructive potential in the vertical direction.[41] To compensate the gravity and form an effective trapping potential, a magnetic field gradient of $\partial B/\partial z = 31.3$ G/cm needs to be applied for the Cs atoms in the $F = 3$, $m_F = 3$ state to cancel the gravity completely, i.e., $\mu_B m_F g_F \frac{\partial B}{\partial z} = mg$, where μ_B is Bohr's magneton, $g_F = -1/4$ denotes the Landé g-factor, and g is the gravitational acceleration. The magnetic field gradient is produced by a pair of quadrupole coils, as shown in Fig. 1(b).

According to Maxwell's equation of $\nabla \cdot B = 0$ and the cylindrical symmetry, the application of $\partial B/\partial z$ leads to the horizontal magnetic field gradient of $\partial B/\partial x = \partial B/\partial y = -1/2\ \partial B/\partial z$, which causes the horizontal outward pointing force and leads to the anti-trapping potential in the horizontal direction. In order to eliminate the influence of the anti-trapping potential along the horizontal direction, we use a vertical bias field B_0, which is produced by another pair of Helmholtz coils shown in Fig. 1(b), to reduce the outward force. The combined field leads to a horizontal trapping frequency

$$\omega_p = \sqrt{\frac{m_F g_F \mu_B}{4mB_0}\left(\frac{\partial B}{\partial z}^2 - 4\varepsilon B_0^2\right)}, \tag{1}$$

where $\varepsilon = 0.0303$ cm^{-2} denotes the departure of the actual geometry of magnetic coils from the Helmholtz configuration.

3. Results

3.1. The 3D degenerated Raman sideband cooling

Cs atoms are slowed down by a Zeeman slower and then collected by a MOT with up to $\sim 5\times10^8$ atoms. Through the compressed MOT and optical molasses cooling, we have 6×10^7 atoms with the temperature of ~ 8 μK. For a lower temperature, we use 3D dRSC to further cool and polarize the atoms in the $F=3, m_F=3$ state. The lattice in 3D dRSC is adiabatically switched on before the end of optical molasses for 0.5 ms, and the depumping laser is simultaneously switched on to keep the atoms populating in the $F=3$ state. The magnetic fields produced by three pairs of compensation coils are adjusted to the optimized values for 2.5 ms previous to the switching of the optical pump laser, because the compensation coils have a 1.5-ms delay. During the cooling process, the atoms are transferred from the $|6S_{1/2}, F=3, m_F, n\rangle$ state into $|6S_{1/2}, F=3, m_F-1, n-1\rangle$ by a two-photon Raman process, and then the atoms are excited by the σ^+ optical pumping laser to the $|6P_{3/2}, F'=2, m_F, n-1\rangle$ state. In the lamb-Dicke regime of $\sqrt{\frac{E_r}{\hbar\omega}} \ll 1$, where E_r is the recoil energy of photon and ω is the vibrational frequency of the lattice in 3D dRSC, the vibrational quantum number is conserved in the spontaneous decay from the excited $|6P_{3/2}, F'=2, m_F, n-1\rangle$ state. The cooling enables that the atoms finally populate in the $|6S_{1/2}, F=3, m_F=2, n=0\rangle$ state, which is a dark state for the σ^+ pumping light with the $6S_{1/2}, F=3 \to 6P_{3/2}, F'=2$ transition. To transfer atoms to the $|6S_{1/2}, F=3, m_F=3, n=0\rangle$ state, the direction of the magnetic field is slightly tilted relative to the optical pumping beam for a weakly π-polarized component.

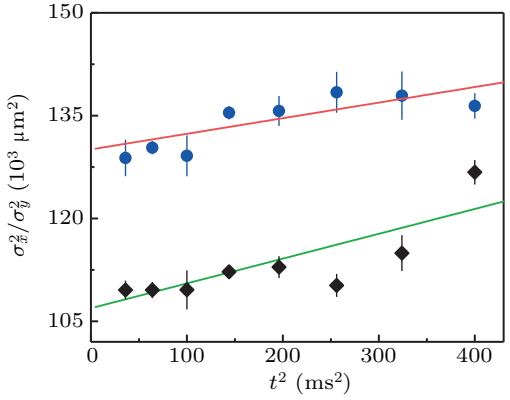


Fig. 2. The square of the measured $1/e$ width of atomic cloud σ_x^2 (blue circles) and σ_y^2 (black diamonds) as a function of the square of flight time t^2. The $1/e$ widths σ_x and σ_y are obtained through the atomic column density distribution along x and y directions, respectively. The temperature of atoms is given by using Eq. (2) to fit the data, and the red and green lines are the corresponding linear fittings.

After the 20-ms dRSC, the optical pumping laser and depumping laser are switched off, and then the lattice laser is adiabatically switched off. The number of atoms is measured as $N=5\times10^7$ by the absorption image. The atomic temperature is determined by fitting the linear dependence of $\sigma_{i,t}^2$ on t^2

$$\sigma_{i,t}^2 = \sigma_{i,0}^2 + \frac{2k_B T_i}{m} t^2, \tag{2}$$

where $\sigma_{i,t}$ is the $1/e$ width of the atomic cloud with subscript i being the x or y direction at the flight time t.[40] The fitted temperature is $T_x = 360\pm120$ nK and $T_y = 580\pm160$ nK, and the corresponding effective temperature is about 480 nK.

We precisely diagnose the magnetic field used in 3D dRSC by the microwave spectroscopy and estimate the atomic population in the $F=3$, $m_F=3$ state. Here a 1-ms microwave pulse is used to pump the atoms in the $6S_{1/2}$, $F=3$ to the $6S_{1/2}$, $F=4$ state, and then the probe laser with the $6S_{1/2}$, $F=4 \to 6P_{3/2}$, $F'=5$ transition is used in the absorption image. Figure 3 shows the dependence of the number of atoms on the frequency of the microwave pulse. In Fig. 3, we find five main peaks and they correspond to the transitions of $F=3$, $m_F=3 \to F'=4$, $m_F'=2$, 3, 4 and $F=3$, $m_F=2 \to F'=4$, $m_F'=1$, 2, 3, where the $F=3$, $m_F=3 \to F'=4$, $m_F'=2$ transition has the same frequency with the $F=3$, $m_F=2 \to F'=4$, $m_F'=3$ transition. Any two adjacent peaks have the same energy spacing, which can be calculated by the Zeeman splitting under an external magnetic field. The transitional energy is given by

$$E_{|F=I\pm1/2, m_F, B\rangle} = -\frac{E_H}{4I+2} + g_I\mu_B B m_F \pm \frac{E_H}{2}\left(1+\frac{4m_F x}{2I+1}+x^2\right)^{1/2}, \tag{3}$$

where $I=7/2$ is the nuclear spin of Cs atoms, $E_H = h\times 9192.63177$ MHz is the hyperfine splitting of the ground state, $g_I = -3.98854\times10^{-4}$ is the nuclear Landé g-factor, $g_J = 2.00254$ is the fine structure Landé g-factor in the $6S_{1/2}$ ground state, and $x = (g_J - g_I\mu_B B)/E_H$.[42] Based on Eq. (3), we calculate the splitting of the Zeeman sublevels induced by an external magnetic field, the effective magnetic field in 3D dRSC is derived for 108 mG. Thus the vibrational frequency of the lattice is determined as $\omega = 2\pi\times50$ kHz according to $\hbar\omega = \Delta m_F \mu_B g_F$ with $\Delta m_F = 1$.

In Fig. 3, the population of atoms in the different Zeeman sublevels indicates that most of the atoms populate in the $F=3$, $m_F=3$ state, and the other atoms mainly populate in the $F=3$, $m_F=2$ state. The number of atoms populating in the $F=3$, $m_F=3$ state is directly estimated as $N \geq 3.5\times10^7$ by referring to the number of atoms detected with the $F=3$, $m_F=3 \to F'=4$, $m_F'=3$ microwave transition. The energy spacing between the two adjacent vibrational levels in the lattice of 3D dRSC defines the lowest temperature of $T=300$ nK, but the obtained effective temperature of

$T \sim 480$ nK is higher than the prediction. This may be attributed to the slight heating in the optical pumping process and the scattering of the photons from the lattice in 3D dRSC. The low temperature prevents the inelastic endothermic collisions of the Cs atoms in the $F = 3$, $m_F = 3$ state and will improve the efficiency of loading the cooled atoms into the magnetically levitated ODT.

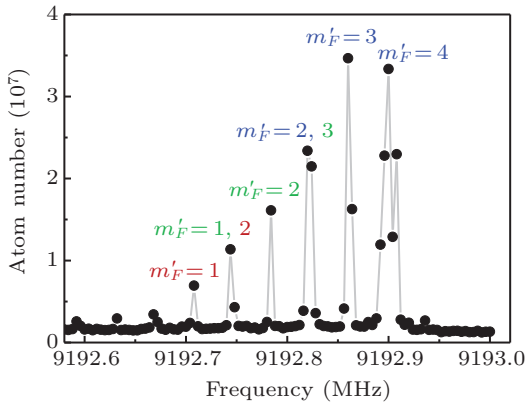


Fig. 3. The number of atoms detected by using a microwave pulse instead of the repumping laser in absorption image as a function of microwave frequency. The peaks represent that the atoms in the sublevels of $F = 3$, $m_F = 1,2,3$ are transferred to the sublevels of $F = 4$, $m'_F = 1,2,3,4$ according to the selection rule of $\Delta m_F = 0, \pm 1$. Dots are from the experimental measurement, and the lines connecting the dots are used to guide the eyes.

3.2. Magnetically levitated optical dipole trap

During the loading of ODT, the magnetic field gradient should be switched on quickly for the formation of an effective trapping potential in the vertical direction. In our experiment, however, the eddy currents in the metal vacuum chamber and other stainless steel flanges limit the rapid variation of magnetic field gradient. When the magnetic force is increasing but has not yet compensated for the gravity completely, the remaining gravitational force always accelerates the atoms and hence leads to the heating of the atomic sample. Thus, to suppress the heating, an excessive levitation gradient of $\partial B/\partial z >$ 31.3 G/cm is used to reduce the velocity obtained by the atoms in the loading process of ODT. When the magnetic field gradient reaches $\partial B/\partial z = 31.3$ G/cm, the atoms have the maximum downward velocity. With the continuous increase of $\partial B/\partial z$, an excessively magnetic force can reduce the downward velocity of atoms. The value of the excessive levitation gradient is optimized experimentally for a fixed duration of 4 ms. As shown in Fig. 4(a), the number of atoms trapped in the ODT first increases and then decreases with the excessive levitation gradient, and an optimized value of $\partial B/\partial z = 40.5$ G/cm is used to maximize the loading of atoms from 3D dRSC into the ODT.

The timing diagram for the magnetically levitated loading of ODT is summarized in Fig. 4(a). When the lattice in 3D DRSC is shut down, the magnetic field gradient is switched on and quickly ramped to an excessive levitation gradient of $\partial B/\partial z = 40.5$ G/cm. After a holding time of 4 ms, the magnetic field gradient takes 2 ms to decrease to $\partial B/\partial z = 31.3$ G/cm. We find that the application of the excessive $\partial B/\partial z$ has the advantages not only for improving the number of atoms loaded into the ODT but also for reducing the heating of atoms. The bias field is ramped to $B = 105$ G within 6 ms to eliminate the horizontal anti-trapping potential induced by the application of the magnetic field gradient.

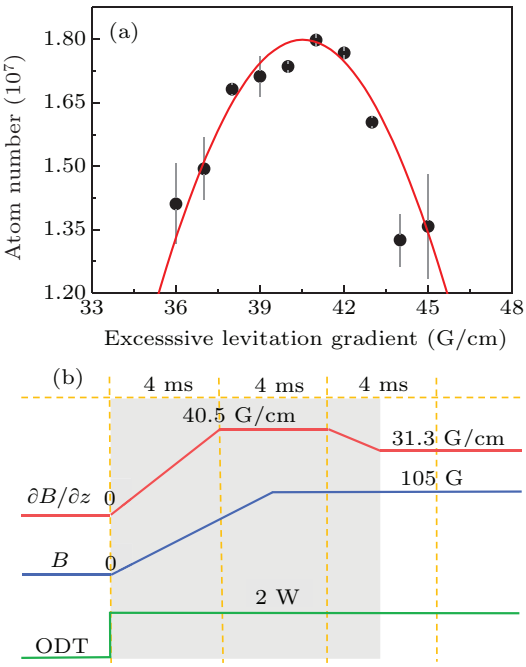


Fig. 4. Optimization for the loading of the magnetically levitated ODT. (a) The number of atoms detected after 200 ms following the loading of the ODT as a function of excessive levitation field. The dots are the experimental data, and the solid line is the Gaussian fitting to guide the eyes. (b) The time sequence of magnetic field gradient $\partial B/\partial z$ and bias field B in the optimized loading of the ODT.

Based on the optimized parameters, we have loaded 1.8×10^7 Cs atoms into the ODT. Here the number of atoms in the ODT is detected by directly imaging the atomic cloud after 200 ms following the loading of ODT. We find that the atomic cloud is heated to about 3 μK after transferring into the ODT. We largely attribute the heating to the imperfect phase space matching. The atomic cloud after 3D dRSC has a $1/e$ of ~ 350 μm, but an equilibrium distribution in the ODT would have a $1/e$ of ~ 100 μm. Besides, the expansion of the atomic cloud in the levitation process leads to the increase of temperature.

3.3. Three-body recombination of atoms in the ODT

For the ultracold Cs atoms in the $|6S_{1/2}, F = 3, m_F = 3\rangle$ state, the three-body recombination is the dominant loss mechanism. As shown in Fig. 5, the number of atoms exhibits a strong three-body loss.[37] In the three-body recombination process, the interacting three particles collide and two of them form a dimmer, and then both the dimmer and the remaining particle escape from the trap.[38,39] The loss rate equa-

tion for the per-particle is given as $\dot{N}/N = -L_3\langle n^2\rangle$, where N is the number of atoms, L_3 is the three-body loss coefficient, and n is the atomic density. When away from unitarity, $L_3 \sim \hbar a^4/m$ with a dimensionless prefactor exhibiting a variation with a in Efimov physics,[43] and a is the s-wave scattering length. According to the atomic density distribution in 3D harmonic trap, the term including the average square density can be directly expressed as $L_3\langle n\rangle^2 = \beta N^2/T^3$ with $\beta = L_3 m^3\overline{\omega}^6/(8\pi^3 k_B^3\sqrt{27})$, and $\overline{\omega}$ denotes the geometrical mean of the trapping frequencies. By considering the collisions of atoms with the background gas as an additional loss term of $-\alpha N$, we obtain a differential equation of the atom number, i.e.,

$$\frac{\mathrm{d}N}{\mathrm{d}t} = -\alpha N - \beta\frac{N^3}{T^3}. \tag{4}$$

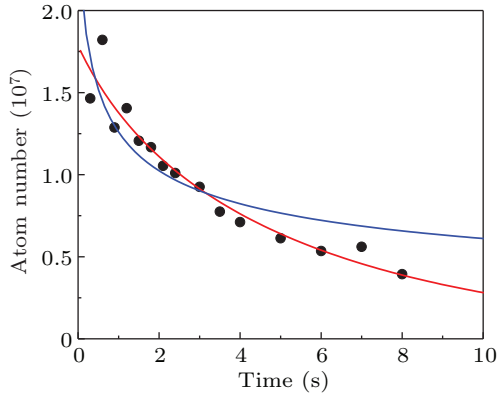


Fig. 5. The number of atoms in the ODT as a function of time. The red line is obtained by using Eq. (8) to fit the data, and the fitted three-body loss coefficient is $L_3 = 7.73\times10^{-25}$ cm^6/s. The blue line is obtained by using Eq. (9) to fit the data, where only the three-body loss is considered. The number of atoms shows a strong three-body loss before the intersection of two fitting curves at ~ 3.1 ms, and after that the one-body loss becomes the dominant mechanism in the atom loss.

At the large scattering length of $a = 1418a_0$, the three-body recombination is so strong that both the dimmer and the third atom are immediately expelled from the trap, and the number of atoms exhibits a large three-body loss. The atoms undergoing three-body recombination have an average potential energy of $k_BT/2$, but the ensemble average is $3k_BT/2$.[37] The loss of an atom leaves an extra energy of k_BT in the remaining ensemble, and this leads to heating. The heating energy corresponding to the relative change in the temperature for the loss of one atom is related to the average energy. The rate of temperature change can be given by multiplying the loss rate of atom number:

$$\frac{1}{T}\frac{\mathrm{d}T}{\mathrm{d}t} = \frac{\dot{N}}{N}\frac{k_BT}{3k_BT}. \tag{5}$$

By replacing the atomic loss rate, the evolution of temperature can be expressed as

$$\frac{1}{T}\frac{\mathrm{d}T}{\mathrm{d}t} = \frac{\beta}{3}\frac{N^2}{T^3}. \tag{6}$$

Using Eq. (6) to substitute the term $\beta N^2/T^3$ in Eq. (4), we can obtain the relationship between N and T as

$$\frac{N}{N_0} = \left(\frac{T_0}{T}\right)^3 \mathrm{e}^{-\alpha t}, \tag{7}$$

where N_0 and T_0 are the number of atoms and the atomic temperature after the loading of the atoms into the ODT. By applying Eq. (7) to Eq. (6), N can be eliminated and the variation of T with t can be deduced analytically. The evolution of the atom number is derived by substituting the solution for T into Eq. (7). The analytical expression of the atom number is given as

$$N(t) = N_0\left(1+\frac{1.5\beta N_0^2}{\alpha T_0^3}(1-\mathrm{e}^{-2\alpha t})\right)^{-1/3}\mathrm{e}^{-\alpha t}. \tag{8}$$

The three-body loss coefficient is derived as $L_3 = 7.73\times10^{-25}$ cm^6/s by using Eq. (8) to fit the experimental evolution of the atom number.

In addition, we try to consider only the three-body loss mechanism in the decay model of the atom number with the negligible collisions of atoms with the background gas, i.e., the one-body loss rate is $\alpha \to 0$ in Eq. (4). Equation (8) can be simplified as

$$N(t) = N_0\left(1+\frac{3\beta N_0^2}{T_0^3}t\right)^{-1/3}. \tag{9}$$

However, Eq. (9) cannot provide an excellent fit for the data, as shown in the blue curve in Fig. 5. Therefore the atom loss induced by their collisions with the background gas has to be taken into account. Two fitting results illustrate that the rate of three-body loss reduces with the decrease of atomic density, and the one-body loss becomes dominant. Our result also indicates the lifetime of atoms in the ODT is finally determined by the one-body loss from the collisions with the background gas.

4. Conclusion

We have used 3D dRSC to cool a large number of atoms to a cold temperature, which enables the loading of more atoms into a crossed ODT. The optimized excessive levitation is used to reduce the atomic velocity induced by the uneliminated gravity after switching off the lattice laser but before the magnetic field gradient reaches to the critical value to completely cancel the gravity. Compared to the loading of an ODT from a bare MOT or the gray-molasses cooling, there is a significant increase in the number of atoms by a factor of ~ 10 and 3, and an decrease in the temperature by a factor of ~ 50 and 5, respectively.

For the optically trapped ultracold Cs atoms, the number of atoms shows a fast decay because of a strong three-body loss at the large scattering length. We study the three-body recombination by analyzing the strong loss of Cs atom, and obtain the three-body loss coefficient by fitting the derived model

to the experimental data. When the atomic density decreases continuously, we find that the one-body loss induced by the collisions of atoms with the background gas becomes dominant in the atom loss. Finally, the lifetime of atoms in the ODT is determined by the one-body loss.

Acknowledgements

Project funded by the National Key Research and Development Program of China (Grant No. 2022YFA1404201), the National Natural Science Foundation of China (Grant Nos. 62020106014, 92165106, 62175140, 12074234, and 11974331), and the Applied Basic Research Project of Shanxi Province, China (Grant No. 202203021224001).

References

[1] Bloch I, Dalibard J and Nascimbène S 2012 *Nat. Phys.* **8** 267
[2] Clark L W, Gaj A, Feng L and Chin C 2017 *Nature* **551** 356
[3] Li J R, Lee J, Huang W J, Burchesky S, Shteynas B, Top F C, Jamison A O and Ketterle W 2017 *Nature* **543** 91
[4] Cooper N R, Dalibard J and Spielman I B 2019 *Rev. Mod. Phys.* **91** 015005
[5] Li Y Q, Zhang J H, Wang Y F, Du H Y, Wu J Z, Liu W L, Mei F, Ma J, Xiao L T and Jia S T 2022 *Light. Sci. Appl.* **11** 13
[6] Wang Y F, Zhang J H, Li Y Q, Wu J Z, Liu W L, Mei F, Hu Y, Xiao L T, Ma J, Chin C and Jia S T 2022 *Phys. Rev. Lett.* **129** 103401
[7] Wang Y F, Du H Y, Li Y Q, Mei F, Hu Y, Xiao L T, Ma J and Jia S T 2023 *Light. Sci. Appl.* **12** 50
[8] Burchianti A, Valtolina G, Seman J A, Pace E, De Pas M, Inguscio M, Zaccanti M and Roati G 2014 *Phys. Rev. A* **90** 043408
[9] Sievers F, Kretzschmar N, Fernandes D R, Suchet D, Rabinovic M, Wu S J, Parker C V, Khaykovich L, Salomon C and Chevy F 2015 *Phys. Rev. A* **91** 023426
[10] Satter C L, Tan S and Dieckmann K 2018 *Phys. Rev. A* **98** 023422
[11] Kim K, Huh S J, Kwon K and Choi J 2019 *Phys. Rev. A* **99** 053604
[12] Colzi G, Durastante G, Fava E, Serafini S, Lamporesi G and Ferrari G 2016 *Phys. Rev. A* **93** 023421
[13] Shi Z L, Li Z L, Wang P J, Meng Z M, Huang L H and Zhang J 2018 *Chin. Phys. Lett.* **35** 123701
[14] Salomon G, Fouché L, Lepoutre S, Aspect A and Bourdel T 2014 *Phys. Rev. A* **90** 033405
[15] Nath D, Easwaran R K, Rajalakshmi G and Unnikrishnan C S 2013 *Phys. Rev. A* **88** 053407
[16] Bruce G D, Haller E, Peaudecerf B, Cotta D A, Andia M, Wu S, Johnson M Y H, Lovett B W and Kuhr S 2017 *J. Phys. B* **50** 095002
[17] Chen H Z, Yao X C, Wu Y P, Liu X P, Wang X Q, Wang Y X, Chen Y A and Pan J W 2016 *Phys. Rev. A* **94** 033408
[18] Rosi S, Burchianti A, Conclave S, Naik D S, Roati G, Fort C and Minardi F 2018 *Sci. Rep.* **8** 1301
[19] Hsiao Y F, Lin Y J and Chen Y C 2018 *Phys. Rev. A* **98** 033419
[20] Kerman A J, Vuletić V, Chin C and Chu S 2000 *Phys. Rev. Lett.* **84** 439
[21] Treutlein P, Chung K Y and Chu S 2001 *Phys. Rev. A* **63** 051401
[22] Weber T, Herbig J, Mark M, Nägerl H and Grimm R 2003 *Science* **299** 232
[23] Kraemer T, Herbig J, Mark M, Weber T, Chin C, Nägerl H and Grimm R 2004 *Appl. Phys. B* **79** 1013
[24] Hung C L, Zhang X B, Gemelke N and Chin C 2008 *Phys. Rev. A* **78** 011604
[25] Wang Y F, Li Y Q, Wu J Z, Liu W L, Hu J Z, Ma J, Xiao L T and Jia S T 2021 *Opt. Express* **29** 13960
[26] Gröbner M, Weinmann P, Kirilov E and Nägerl H 2017 *Phys. Rev. A* **95** 033412
[27] Hu J Z, Urvoy A, Vendeiro Z, Crépel V, Chen W L and Vuletić V 2017 *Science* **358** 1078
[28] Solano P, Duan Y H, Chen Y T, Rudelis A, Chin C and Vuletić V 2019 *Phys. Rev. Lett.* **123** 173401
[29] Grimm R, Weidemüller M and Ovchinnikov Y B 2000 *Adv. At. Mol. Opt. Phys.* **42** 95
[30] Shiddiq M, Ahmed E M, Havey M D and Sukenik C I 2008 *Phys. Rev. A* **77** 045401
[31] Olson A J, Niffenegger R J and Chen Y P 2013 *Phys. Rev. A* **87** 053613
[32] Chin C, Grimm R, Julienne P and Tiesinga E 2010 *Rev. Mod. Phys.* **82** 1225
[33] Fletcher R J, Gaunt A L, Navon N, Smith R P and Hadzibabic Z 2013 *Rev. Lett.* **111** 125303
[34] Makotyn P, Klauss C E, Goldberger D L, Cornell E A and Jin D S 2014 *Nat. Phys.* **10** 116
[35] Eigen C, Glidden J A P, Lopes R, Navon N, Hadzibabic Z and Smith R P 2017 *Phys. Rev. Lett.* **119** 250404
[36] Gao C, Sun M Y, Zhang P and Zhai H 2020 *Phys. Rev. Lett.* **124** 040403
[37] Weber T, Herbig J, Mark M, Nägerl H and Grimm R 2003 *Phys. Rev. Lett.* **91** 123201
[38] Rem B S, Grier A T, Ferrier-Barbut I, Eismann U, Langen T, Navon N, Khaykovich L, Werner F, Petrov D S, Chevy F and Salomon C 2013 *Phys. Rev. Lett.* **110** 163202
[39] Eismann U, Khaykovich L, Laurent S, Ferrier-Barbut I, Rem B S, Grier A T, Delehaye M, Chevy F, Salomon C, Ha L and Chin C 2016 *Phys. Rev. X* **6** 021025
[40] Ketterle W, Durfee, D S and Stamper-Kurn D M 1999 in *Proc. Int. School of Physics* "Enrico Fermi" p. 67
[41] Jenkina D L, McCarron D J, Koppinger M P, Cho H W, Hopkins S A and Cornish S L 2011 *Eur. Phys. J. D* **65** 11
[42] Steck D A 2003 *Cesium D line data*
[43] Kraemer T, Mark M, Waldburger P, Danzl J G, Chin C, Engeser B, Lange A D, Pilch K, Jaakkola A, Nägerl H and Grimm R 2006 *Nature* **440** 315